Performance of the Large Hadron Collider cleaning system during the squeeze: Simulations and measurements

S. Tygier,[1,2,*] R. B. Appleby,[1,2] R. Bruce,[3] D. Mirarchi,[3] S. Redaelli,[3] and A. Valloni[1,3]

[1]*The University of Manchester, Oxford Road, Manchester M13 9PL, United Kingdom*
[2]*The Cockcroft Institute, Daresbury WA4 4AD, United Kingdom*
[3]*CERN, 1217 Meyrin, Geneva, Switzerland*

(Received 13 July 2018; published 7 February 2019)

The Large Hadron Collider (LHC) at CERN is a 7 TeV proton synchrotron, with a design stored energy of 362 MJ per beam. The high-luminosity (HL-LHC) upgrade will increase this to 675 MJ per beam. In order to protect the superconducting magnets and other sensitive equipment from quenches and damage due to beam loss, a multilevel collimation system is needed. Detailed simulations are required to understand where particles scattered by the collimators are lost around the ring in a range of machine configurations. Merlin++ is a simulation framework that has been extended to include detailed scattering physics, in order to predict local particle loss rates around the LHC ring. We compare Merlin++ simulations of losses during the squeeze (the dynamic reduction of the β function at the interaction points before the beams are put into collision) with loss maps recorded during beam squeezes for run 1 and 2 configurations. The squeeze is particularly important, as both collimator positions and quadrupole magnet currents are changed. We can then predict, using Merlin++, the expected losses for the HL-LHC to ensure adequate protection of the machine.

DOI: 10.1103/PhysRevAccelBeams.22.023001

I. INTRODUCTION

The LHC collimation system [1,2] is designed to protect the ring from normal beam losses caused by diffusion and scattering, as well as abnormal fast losses. In order to achieve this, it uses a multistage system for betatron cleaning, installed in insertion region 7 (IR7), and a similar but reduced system for momentum cleaning installed in IR3. The main components are shown in Fig. 1. The primary collimators (TCPs) are made of carbon-fiber composites (CFCs) and sit closest in to intercept the beam halo. The secondary collimators (TCSs), also CFCs and shower absorbers (TCLAs) made of tungsten, absorb the deflected protons and secondary particles. There are also tungsten tertiary collimators (TCTs) that provide extra protection for the experiments, as well as TCLs to absorb collision debris. About 150 m upstream of each experiment, a pair of one horizontal (TCTPH) and vertical (TCTPV) TCT is installed. The LHC's multistage collimation system has proved to be performing reliably during run 1 (2010–2012) with beam energies of 3.5 and 4 TeV and the start of run 2 (2015–2018) at 6.5 TeV. However, the future physics program at 7 TeV and the higher intensities of HL-LHC [3,4] provide new challenges, so it is important that the performance is well understood and can be accurately simulated. The HL-LHC program includes upgrades to the collimation system such as new collimators, new jaw materials [5], and new embedded instrumentation [6].

In this article, we present predictions for HL-LHC losses during luminosity leveling, as well as measurements of the performance of the LHC collimation system during runs 1 and 2. Previously, studies of LHC collimation efficiency have been successfully performed using the SixTrack code with comparisons to beam loss monitor (BLM) data at fixed

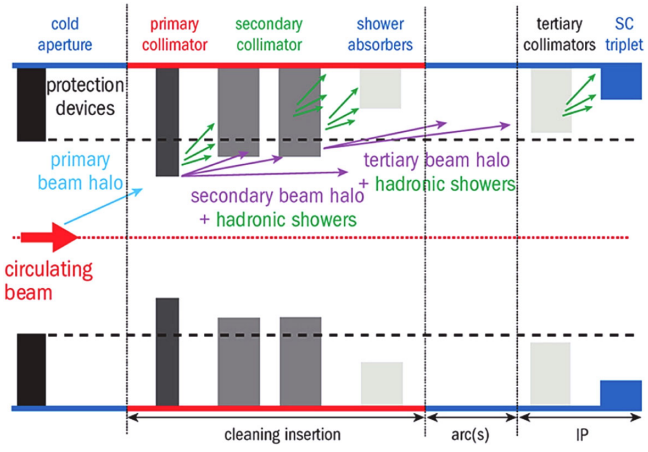

FIG. 1. Overview of the main components involved in the multistage collimation system.

*sam.tygier@manchester.ac.uk

optical configurations [7–15]. These demonstrate that maps of proton loss locations are useful for evaluating collimation scenarios and as input to energy deposition studies using codes such as FLUKA [16]. In this article, we use instead the code Merlin++, which is described in Sec. II, and present the first comparison loss maps taken during the squeeze. In Sec. III, the BLMs [17,18] are described. These are used to validate the simulation code. This system consists of about 4000 ionization chambers distributed around the ring to monitor losses at critical elements.

For this work, we consider the slow losses that occur during normal operation of the LHC. Particles in the core of the beam can be excited to higher amplitudes by a number of effects, drifting out to form the beam halo. When a particle's amplitude is large enough, it is intercepted by the collimators.

Before bringing the LHC beams into collision, they must first be ramped from the injection energy (450 GeV) to full energy (6.5 TeV in run 2) and the β^* [the β function at the experiment interaction points (IPs)] reduced. This latter part of the operational cycle is called the squeeze. In run 1, these actions were performed separately; however, during run 2, a combined ramp and squeeze sequence was introduced to reduce the cycle duration. Figure 2 shows the beam modes for a typical run 1 production fill, from injection of the physics beam through to stable beams for physics production. In Fig. 2, the squeeze begins at around 3500 s, with the β^* at IP 1/5 being reduced from 11 to 0.6 m.

The squeeze is an important time for the collimation system, as there are dynamic changes to the machine optical configuration and collimator positions, while the stored energy in the beam is at its maximum. It also provides a good opportunity to validate a simulation against measurements in a range of configurations, allowing investigation into any differences found.

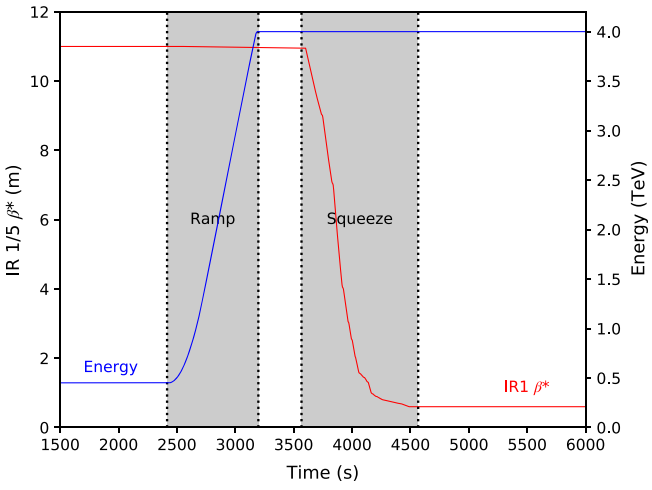

FIG. 2. β^* in IR 1/5 and beam energy during a typical squeeze during 2012, showing the ramp and squeeze periods.

Sections IV and V compare the simulations to data for runs 1 and 2, respectively. This gives us the confidence in Merlin++'s particle tracking and scattering models, in order to use it for making predictions of future configurations. In Sec. VI, we evaluate the loads on the collimators in the HL-LHC, for the most pessimistic loss scenario allowed at full energy. This corresponds to a 0.2 h beam lifetime over 10 s [19,20], giving a total loss power of about 1 MW.

II. CALCULATION OF BEAM LOSSES

To calculate the losses in an accelerator, we must model the trajectories of particles in the magnetic lattice and also the passage and scattering of particles in the materials that make up the collimators.

Merlin++ [21], previously known as MERLIN, is a modular object-oriented accelerator simulation framework, featuring 6D thick lens tracking. Initially developed for the International Linear Collider's beam delivery systems [22], it has since been extended to support synchrotrons. It is written in C++ and can be easily extended by the user, for example, to add new physics models. It has multiprocessor support using the message passing interface protocol for communication; however, for noncollective effects as used in collimation studies, it is more convenient to run multiple independent processes and sum the results.

The user-created program calls the Merlin++ library in order to define a beam line, add appropriate physics processes, create a beam, and then initiate tracking. In these studies, the MADInterface module was used to read in a lattice description from a MADX [23] optics calculation. Machine apertures and collimator gaps were similarly defined in separate files.

While the codes SixTrack [7] and FLUKA have been used for similar comparisons to BLM data previously [11] it is useful to have multiple independent simulation codes in order increase confidence and constrain systematic uncertainness. Merlin++ features thick lens tracking compared to SixTrack's thin lens method and more advanced scattering model as described below. Merlin++ also has some technical advantages; for example, its modular C++ design simplifies the incorporation of new physics models.

The scattering physics used to model the passage of protons through material has recently been upgraded [24]. It contains advanced models of the following processes: multiple Coulomb scattering; ionization based on Landau theory; Rutherford scattering; a new elastic scattering model; and a new single-diffraction dissociation model. The model uses proton-nucleon scattering based on the Donnachie and Landshoff (DL) description of Pomeron and Reggeon exchange and has been fitted to elastic and diffractive scattering data from a large number of previous experiments. The development and implementation of these models are described in detail in our earlier paper [25]. This model has now been included into the Pythia event generator, under the name ABMST model [26]. These new scattering

models give different predictions for losses around the ring compared to the K2 model in older versions of SixTrack; specifically, the single diffractive model was found to cause a significant shift of losses from cold to warm regions. For performance reasons, only the leading proton from each interaction is modeled, equivalent to assuming that the secondaries deposit their energy close to the interaction.

To simulate loss maps, we use an approach similar to earlier LHC studies [10,11]. We track 10^8 protons for 200 turns. The initial particle bunch is generated at the face of the primary collimator in the excitation plane. This simulated bunch is a ring in phase space in the excitation plane that intersects the collimator jaw by 1 μm from its edge, the impact parameter, and Gaussian in the opposite plane. It is prefiltered so that every proton interacts with the primary collimator on the first turn. This saves significant computer resources compared to modeling the real LHC bunch distribution and the diffusion of particles from the core of the bunch. As the beam is tracked, it is compared to the machine aperture at each element. If a proton hits the aperture in a collimator, then it is scattered according to the process cross sections. If the proton hits the aperture of other lattice elements, it is considered as lost at this location. The loss map records the location of every proton loss with a resolution of 10 cm.

The primary collimators are set to be the tightest aperture restriction in the machine so that they are the first material that a proton with sufficient amplitude will hit. The protons that scatter without being absorbed will go on to hit other elements in the ring. If all protons hitting the primary collimator were absorbed by the collimation system, we would consider it to have 100% cleaning efficiency. In practice, we typically see about 8% of protons absorbed during a single pass through a TCP due to inelastic collisions or losing over 95% of their initial energy, which is considered to be a loss. Over subsequent turns around the ring, most protons will be lost in the TCPs. To produce a loss map, which shows the distribution of losses around the ring, we measure the proton loss locations and use them to calculate the local cleaning inefficiency. The simulated local cleaning inefficiency η_{loc} is given by the ratio of particles lost on a given section, N_{loc} (either an element or bin along the S coordinate), to particles lost in the primary collimators, N_{tot}, normalized to the length of the section, Δs, to make the value independent of bin size, i.e.,

$$\eta_{\mathrm{loc}} = \frac{N_{\mathrm{loc}}}{N_{\mathrm{tot}}\Delta s}. \tag{1}$$

The local cleaning inefficiency can then be multiplied by the total beam loss rate to find the local proton loss rate.

III. LOSS MEASUREMENTS

The LHC BLM system uses ionization chamber charged particle detectors to measure the radiation levels around the LHC ring [17,18]. They are used during operation to trigger a beam dump if loss thresholds are exceeded. They also provide continuous measurements of normal beam loss around the ring during the LHC operations and are used to record beam loss during the validation campaigns of the collimation system, when artificial losses are induced with safe low-intensity beams to assess the system response.

To generate a loss map, one of the beams is excited in a given plane using the transverse dampers (ADTs), and the losses are recorded [27]. This allows a clean loss map for an individual beam and plane to be made. Measured LHC loss maps have been studied previously in Refs. [11,15].

During 2012, several loss maps were recorded at 4 TeV in the flattop and fully squeezed optics configurations. No deliberate loss maps were made with the intermediate squeeze optics at 4 TeV, but, as the BLM signals are recorded continuously, it is possible to look at the natural losses during the squeeze. In 2016, at 6.5 TeV, loss maps were generated at the intermediate squeeze points as well as the end points.

These loss maps are crucial to validate simulations, to ensure a good understanding of the collimation system, and hence to demonstrate the performance of the HL-LHC layout. In the following sections, we show the validation for runs I and 2 of the LHC.

IV. RUN 1: 4 TeV

A. Run 1 LHC 2012 configuration

In this article, we investigate losses at intermediate optics points while the machine is in the squeeze mode. Here the optics configurations are changing as a function of the time; see Fig. 2. As β^* is reduced, the β function in the inner triplets must increase, as shown in Fig. 3. Table I shows the optics settings for the squeeze during 2012.

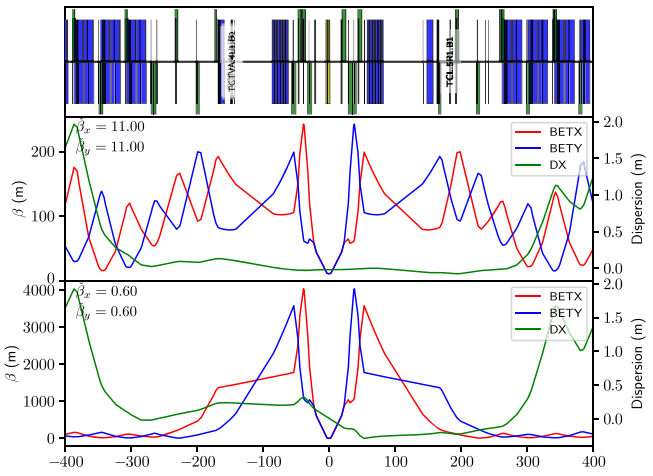

FIG. 3. β functions and dispersion at the ATLAS experiment for flattop (top) and squeezed (bottom) settings for the 2012 run configurations.

TABLE I. Optics settings for the squeeze in 2012 at 4 TeV. The crossing angle can be in the horizontal (H) or vertical (V) plane. Note that, for IR2 and 8, the external crossing angle, applied on top of the spectrometers and their compensation bumps, is given.

	β^* (m)	Half crossing angle (μrad)
ATLAS (IP1)	$11 \rightarrow 0.6$	−145 V
CMS (IP5)	$11 \rightarrow 0.6$	145 H
ALICE (IP2)	$10 \rightarrow 3.0$	−90 V
LHCb (IP8)	$10 \rightarrow 3.0$	−220 H

As well as the optics configuration changing during the squeeze, the TCTs are also in motion. The collimators are set in units of beam sigma, so, as the beam envelope at the collimator's location changes, the collimator jaws are adjusted. Also, the TCTs at the experiments are brought into their tightest position only during the squeeze as the normalized triplet aperture reduces, so their jaw gap in sigma units is decreased during the squeeze, as shown in Table II. We therefore concentrate this study on the losses at the TCTs.

B. Simulated loss maps

Loss maps were simulated in Merlin++ at eight points within the squeeze covering β^* at IP1 and IP5 from 11 to 0.6 m. A bunch of 10^8 protons were tracked for 200 turns. This is sufficient to give good statistics for all relevant collimator and ring losses, even for particles that survive for multiple turns after their first scatter.

Figure 4 shows examples of the loss maps at three of the optical configurations. The highest losses occur on the TCPs in IR7 at around 20 000 m from IR1 as expected and then lower losses along the cleaning hierarchy. Also, significant losses at the momentum cleaning collimators in IR3, at around 7000 m, are observed. The losses at the TCTs in front of the experiments in IR1/2/5/8 do not appear until the later stages of the squeeze. The main cold losses are in the IR7 dispersion suppressor, which is the bottleneck in terms of local cleaning inefficiency.

TABLE II. Collimator settings for the squeeze in 2012 at 4 TeV, from 11 to 0.6 m at IP 1/5, using a normalized beam emittance of 3.5 μm.

Region	Type	Gap (σ)
IR7	TCP	4.3
IR7	TCS	6.3
IR7	TCLA	8.3
IR3	TCP	12.0
IR3	TCS	15.6
IR3	TCLA	17.6
IR1	TCT	$26.0 \rightarrow 9.0$
IR5	TCT	$26.0 \rightarrow 9.0$
IR2	TCT	$26.0 \rightarrow 12.0$
IR8	TCT	$26.0 \rightarrow 12.0$

C. Measured squeeze losses in 2012

As there were no dedicated loss maps made during 2012 at the intermediate squeeze optics settings, we compare to the BLM measurements made during normal LHC operation. These have a number of disadvantages over the dedicated loss maps. They have lower signal levels and so a lower signal to noise ratio. This makes it hard to get clean data in lower loss regions. They contain an unquantified mix of losses from both beams and in both planes. This makes it impossible to completely separate out different sources of loss as can be done with the dedicated loss maps.

The logging database is used to identify typical data-taking fills, where the squeeze was successful and the beam reached the "stable beams" mode. Then the BLM signals and optical parameters as functions of the time can be retrieved for those fills. Even with no losses occurring, there is a continuous low level of background noise recorded by the BLMs. We consider this noise floor to be the limit to the precision of the BLM signal and hence the uncertainty. For each BLM, a background noise level is calculated by averaging the lowest five readings during the squeeze. This value can then be used as an estimate of the uncertainty of the BLM signal.

During a fill, the rate of loss varies considerably. For much of the time, the losses at the TCTs are below the noise thresholds of the BLMs. This can cause spurious values for local inefficiency. It was found that there could be large swings in the total loss rate around the fixed points of the squeeze, so BLM data taken at those points are particularly unreliable.

In order to get a good measure of inefficiency, we identified points in time where the total losses were high enough that the TCT BLMs were above the noise. A peak-finding algorithm was used to find the highest values of the TCT losses within each fill. These points were retained if at the same time stamp there was also a high BLM value at TCP. Figure 5 shows how, for four fills, time stamps with simultaneous peaks are selected. These points were then ranked by the product of the TCT and TCP values and the highest kept.

The BLM signals during regular operation contain a mix of both horizontal and vertical losses. These can be partially separated by looking at the ratios between the vertical, horizontal, and skew TCPs, labeled D6L7, C6L7, and B6L7, respectively, due to their positions in the lattice. A schematic of their layout is shown in Fig. 6. Vertical excitations will hit D6L7, leaving a BLM signal there, but the shower will also leave a signal at C6L7 and B6L7. Horizontal excitations will pass through D6L7 and hit C6L7 first, with the shower peaking in B6L7. We find that cutting on the D6L7 to C6L7 ratio being less than 0.1 and the C6L7 to B6L7 ratio being less than 0.5 selects cases that

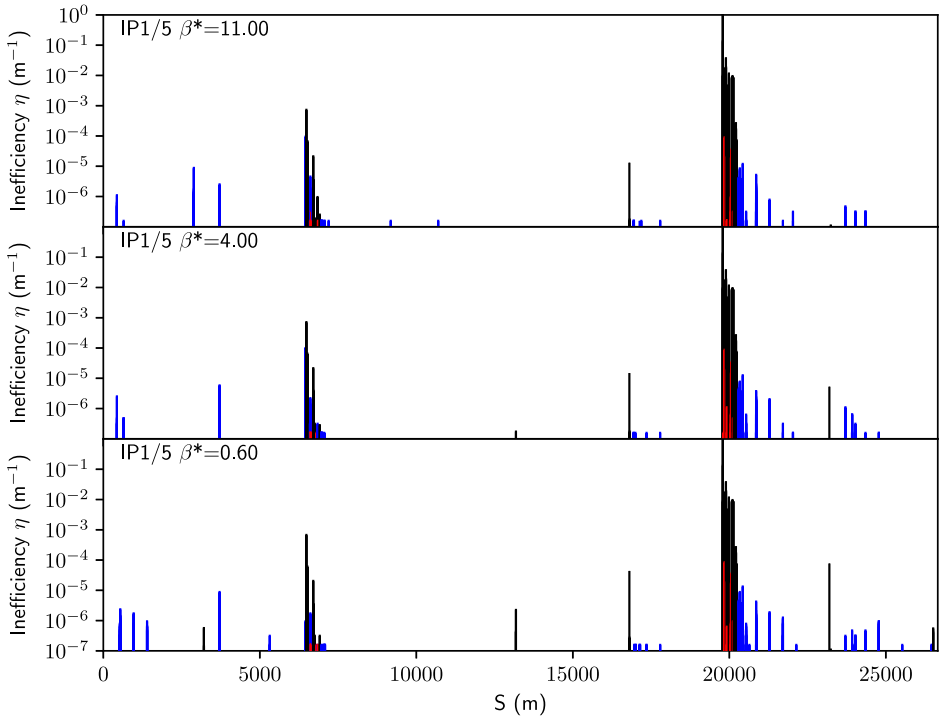

FIG. 4. Loss maps, as simulated with Merlin++ for initial losses in the horizontal plane, for beam 1, made at different points in the squeeze with β^* of 11, 4, and 0.6 m, for the 2012 4 TeV configuration. Losses in collimators are shown in black, in cold magnets in blue, and in warm magnets in red.

are dominated by horizontal losses. This results in 13 data points that pass the filters, covering a range of β^* values from 2 to 0.6 m.

More sophisticated machine-learning algorithms exist to categorize losses [28]; however, these were not used, as they have not been trained on 2012 data.

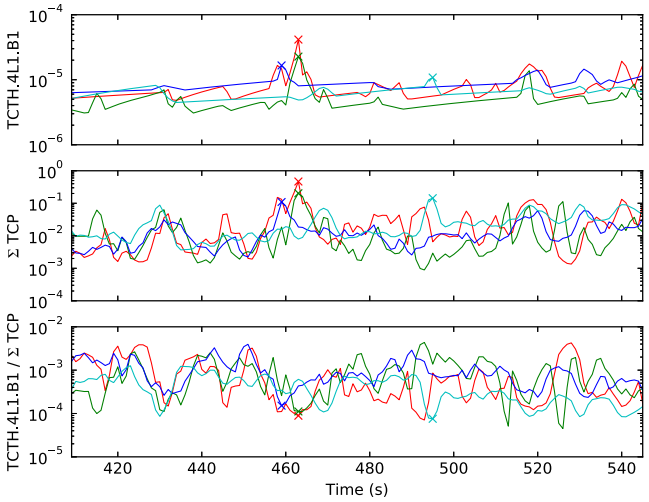

FIG. 5. Peaks in the TCT (top) and TCP (middle) BLM signals are identified for four fills (shown in different colors). At these time steps, the noise on the ratio (bottom) is minimized and so can be taken to get the local cleaning inefficiency.

For the points that pass both filters, we calculate the inefficiency at the TCTs and take the β^* value that corresponds to the time stamp.

D. Comparison between simulation and measurements

First, we can compare the full loss maps taken at the end of the squeeze with IR1/5 β^* of 60 cm. BLM loss maps are from fill 2788 on 1 July 2012. Figure 7 shows losses around the full ring for horizontal beam 1 excitation. Merlin++

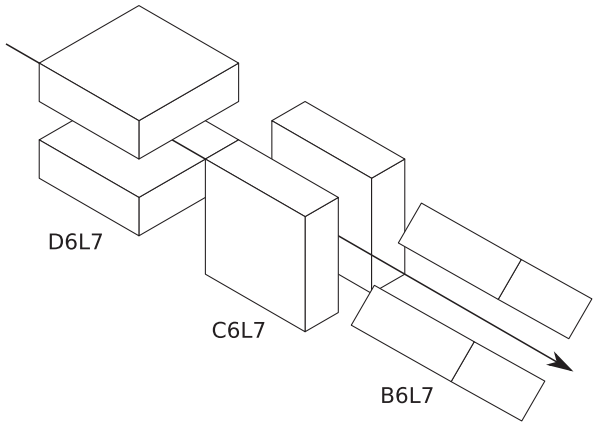

FIG. 6. The three primary collimators at D6L7, C6L7, and B6L7 are oriented to collimate in the vertical, horizontal, and skew planes, respectively. The codes refer to the positions in the sixth cell left of IR7.

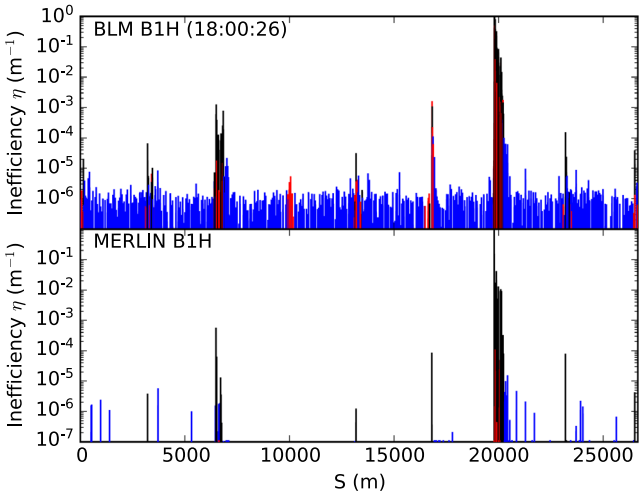

FIG. 7. Beam 1 horizontal loss map from BLMs (top) and Merlin++ (bottom) at 4 TeV with β^* of 60 cm.

reproduces the significant loss peaks in the collimation regions and other IRs. Figure 8 shows the loss map zoomed to the IR7 collimation region. The hierarchy of losses from the TCPs through to the TCSs and TCLAs can be seen in both the simulation and the data. The BLM signal outside the collimators is higher than in the simulation, especially in the warm losses represented by the red bars, as full showers of secondary particles are not simulated in Merlin++. The noise level of the BLMs can be seen in the measurements at around 10^{-6}; these are not real losses and therefore set the precision of the measurement.

While Merlin++ counts the particle losses on the beam pipe, the BLMs record the dose from the radiation shower outside the accelerator's physical components. At LHC energies, the shower from proton impacts has an effective length of approximately 1 m in typical metals with a tail

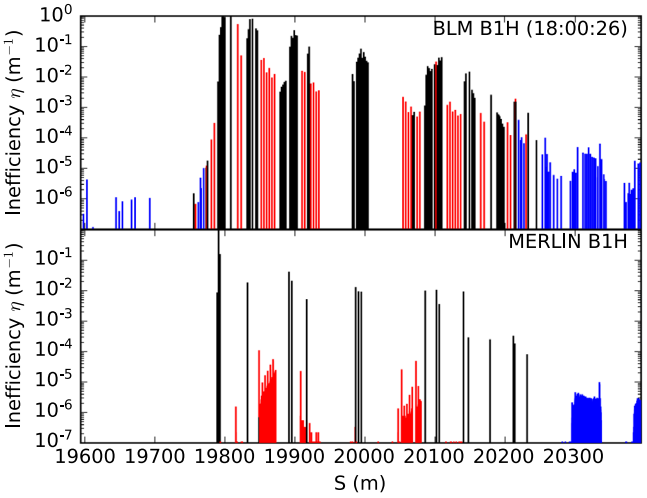

FIG. 8. IR7 beam 1 horizontal loss map from BLMs (top) and Merlin++ (bottom) at 4 TeV with β^* of 60 cm.

expanding up to 10 m [29], so proton losses at one element will also cause a signal in the BLMs at downstream elements. The materials of the magnets and surrounding equipment will absorb some of the energy of the shower. For a full quantitative comparison to the BLM signals, one would need to use the proton loss maps from Merlin++ as inputs to an energy deposition code such as FLUKA. This would be used to model the evolution of the particle showers through the machine elements and the signal response of the BLM ionization chamber. Similar studies using loss maps produced with SixTrack have been demonstrated in Ref. [11].

We can now compare the TCT inefficiency predicted in the Merlin++ simulation with the measurements. In both cases, we are interested in the normalized local cleaning inefficiency at the TCTs, i.e., the ratio of the individual TCT to the total TCP losses. This partially normalizes out the conversion of proton losses to BLM signal values. However, we must also make a normalization to take into account the response of the BLM to the local proton loss and cross talk due to secondary particles from one element reaching the BLM of another. To do this, we normalize to the inefficiency at the fully squeezed configuration. This normalization point is chosen as it has the highest losses and so the lowest statistical error. With the chosen normalization, the different optics configurations can be compared in relative, although not in absolute, assuming that the BLM response is independent of optics.

Figure 9 shows the Merlin++ simulation compared to the data points extracted from the BLM data. As before, BLM error bars are based on the background level found by averaging the five lowest readings within the time window. While the trend is compatible, it is clear that the BLM data are too limited to draw conclusions. The signal to noise ratio in the BLM data is too low for β^* above 2 m to retrieve

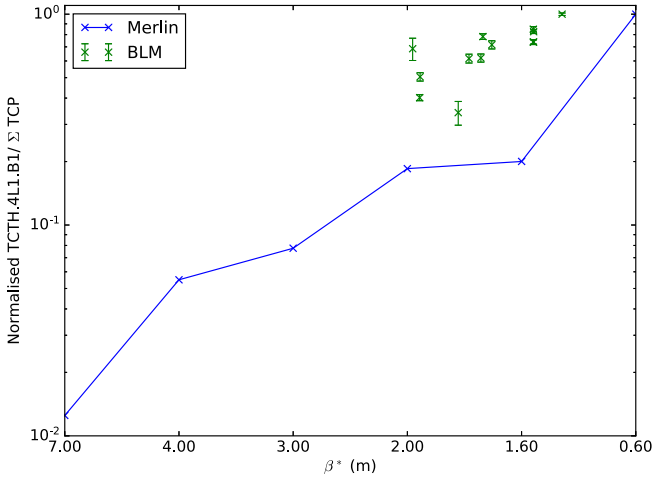

FIG. 9. Comparison between normalized losses in Merlin++ and BLM signal for the horizontal collimator in IR1 (TCTH.4L1.B1) during the squeeze. Note that no losses were seen at the TCT in the simulation for β^* greater than 7 m.

TABLE III. Optics settings for the 2016 squeeze at 6.5 TeV. As before, for IR2 and 8 the external crossing angle is given.

	β^* (m)	Half crossing angle (μrad)
ATLAS (IP1)	3.0 → 0.4	−185 V
CMS (IP5)	3.0 → 0.4	185 H
ALICE (IP2)	10 → 10	200 V
LHCb (IP8)	6.0 → 3.0	−250 H

any data points and give a significant data spread above 1 m. It is clear that dedicated loss maps are needed to make a better comparison.

V. RUN 2: 6.5 TeV

A. Run 2 2016 LHC configuration

Run 2 of the LHC began in 2015 and incorporated changes to the machine configuration, most notably an increase in the beam energy from 4 to 6.5 TeV. In order to reduce the time from injection to collision, a combined ramp and squeeze program was used starting from 2016, such that the initial squeeze, down to β^* of 3 m at IR1 and IR5, happens simultaneously with the energy ramp. Therefore, the squeeze beam mode covers just the final 3–0.4 m of squeezing.

Table III shows the optical parameters for the IPs used during 2016 data taking. Table IV shows the collimation settings used.

B. Measured squeeze losses in 2016

During the 2016 beam commissioning, a number of loss maps were made during the squeeze. This gives a better signal to noise ratio and allows separation of losses from each beam and plane. The maps used in this article were taken on 20 April 2016, during fill 4832. A beam of low-intensity pilot bunches was injected and ramped to 6.5 TeV. During the squeeze, the ADTs for each combination of horizontal and vertical, and beam 1 and 2, were fired in turn to excite one of the bunches in that plane, as shown in Fig. 10, and the BLM signal was recorded [30].

TABLE IV. Collimator settings for the squeeze in 2016 at 6.5 TeV, using a normalized beam emittance of 3.5 μm.

Region	Type	Gap (σ)
IR7	TCP	5.5
IR7	TCS	7.5
IR7	TCLA	11.0
IR3	TCP	15.0
IR3	TCS	18.0
IR3	TCLA	20.0
IR1	TCT	23.0 → 9.0
IR5	TCT	23.0 → 9.0
IR2	TCT	37.0
IR8	TCT	23.0 → 15.0

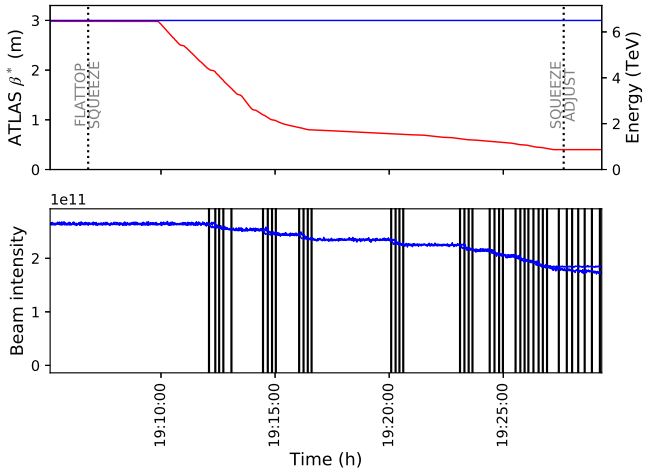

FIG. 10. Loss map recording during fill 4832. The top plot shows the energy (blue) and IR1 β^* (red). The bottom plot shows the fall in beam intensity as each of the four ADTs (for each beam and plane) are fired (vertical lines).

For each BLM, we calculate a background level, by averaging the signal during a 10 s window near the start of the squeeze where losses are low. This fixed value per BLM is used as an estimate of the uncertainty of that BLM's signal during excitation. Note that the background measurement is usually taken closer to the loss map excitation; however, in this case where loss maps are made in rapid succession, this is not possible. There are a number of additional parameters not under control that can contribute to errors, such as orbit shifts and changes in the squeeze rate.

C. Comparison between simulation and measurements

First, we compare a full loss map from fill 4832 taken close to when the β^* at IR1/5 crossed 50 cm. Figures 11 and 12 show full ring and IR7 loss maps comparing BLM

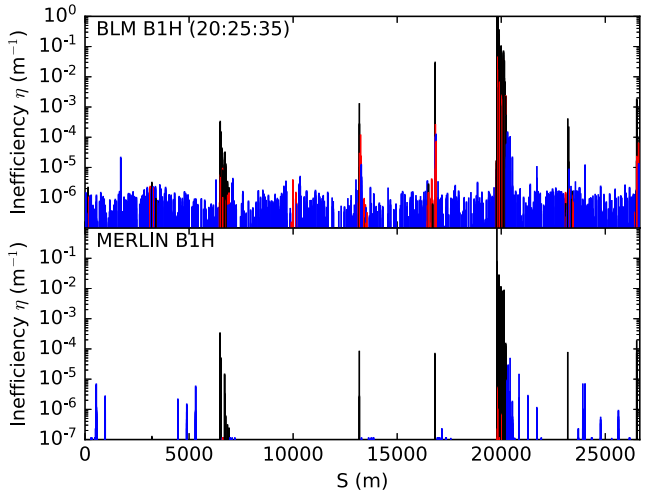

FIG. 11. Beam 1 horizontal loss map from BLMs (top) and Merlin++ (bottom) at 6.5 TeV with β^* of 50 cm.

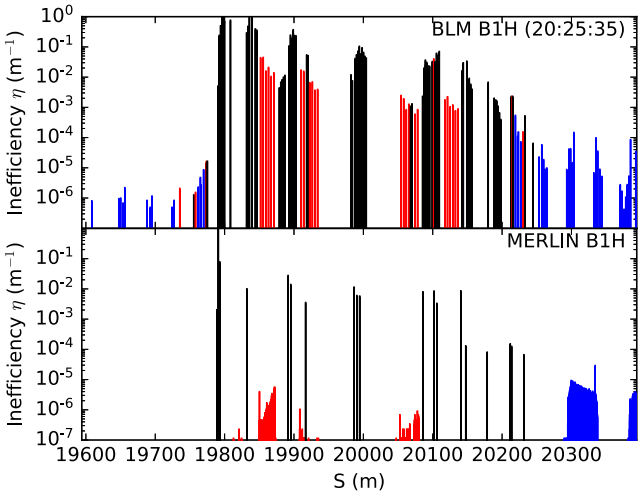

FIG. 12. IR7 beam 1 horizontal loss map from BLMs (top) and Merlin++ (bottom) at 6.5 TeV with β^* of 50 cm.

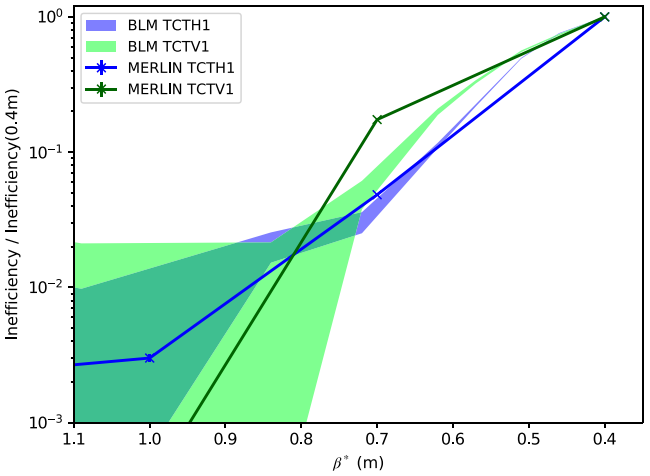

FIG. 14. Enlarged plot of the BLM signal and Merlin++ simulated losses on IR1 TCTs for horizontal excitation. The solid area shows uncertainty bands due to the detector background.

data and Merlin++ simulation. As with the 4 TeV comparisons, we see that Merlin++ reproduces well the main loss locations around the ring and the collimation hierarchy in IR7 well.

We can now compare the normalized cleaning efficiency as a function of β^* between BLM data and Merlin++. In the BLM measurements, during the squeeze we have 11 loss maps in the horizontal plane and nine in the vertical. In the simulations, we have used five different optical configurations.

Figures 13 and 15 show losses on the IR1 TCTs during the squeeze due to horizontal and vertical excitation of the beam. Figures 14 and 16 show enlarged sections of the plot so that more detail is visible at low β^*. Horizontally, we see excellent agreement between the data and simulation, with steep increases in TCT losses as the beam is squeezed to β^* of 0.4 m. For vertical excitation, we again see good overall agreement, although no losses are observed on TCTPV.4L1.B1, the vertical TCT in IR1, in the simulation above β^* of 0.8 m. At larger β^* values, the signals on the TCT BLMs are below the noise levels, so we are not able to record the losses.

Figures 17 and 19 show losses on the IR5 TCTs due to horizontal and vertical excitation of the beam. Again, we show enlarged sections for low β^* in Figs. 18 and 20. For horizontal excitation, we see good agreement for TCTPH.4L5.B1 but higher losses in the simulation for TCTPV.4L5.B1 than in the BLM data. For vertical excitation, Merlin++ reproduces the losses well.

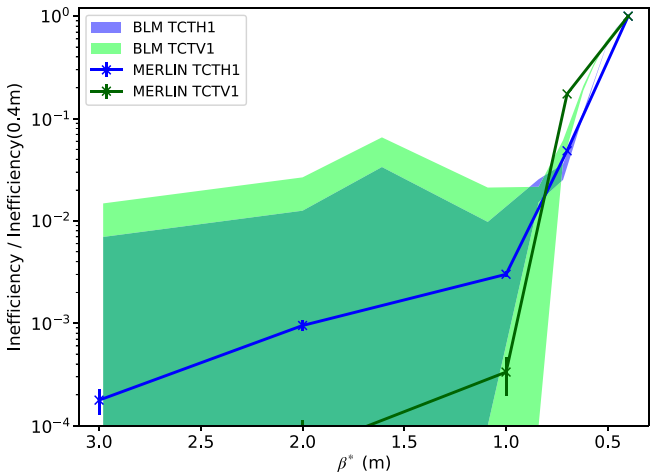

FIG. 13. The BLM signal (shown as uncertainty bands) and Merlin++ simulated losses (shown as solid lines) on IR1 TCTs for horizontal excitation. The solid area shows uncertainty bands due to the detector background.

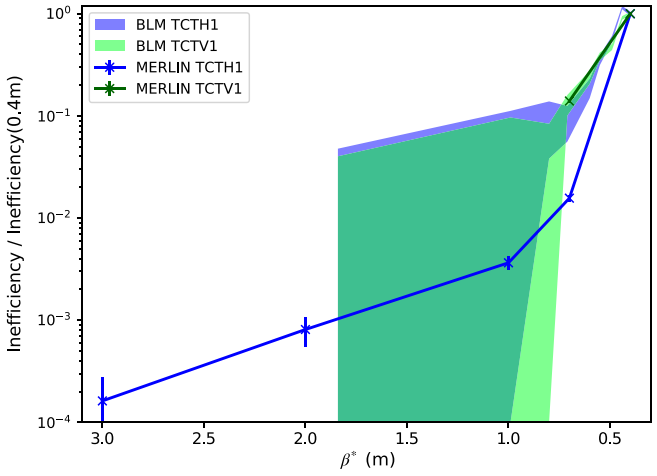

FIG. 15. The BLM signal and Merlin++ simulated losses on IR1 TCTs for vertical excitation. Note that no losses were seen on the vertical TCT at β^* greater than 0.8 m in the simulation or on either TCT at β^* greater than 1.9 m in the data.

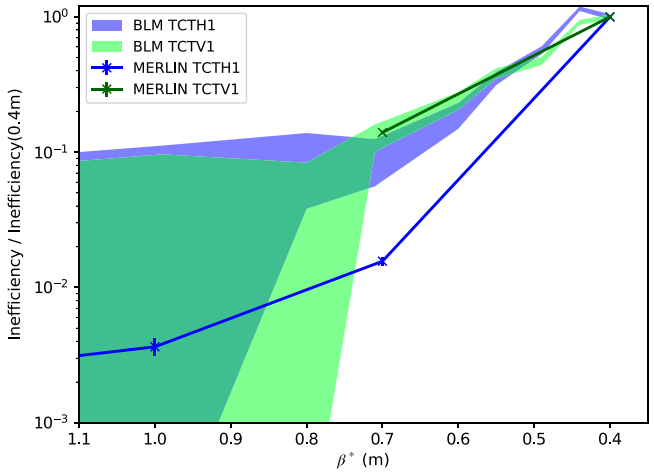

FIG. 16. Enlarged plot of the BLM signal and Merlin++ simulated losses on IR1 TCTs for vertical excitation.

To investigate the loss falloff on TCTPV.4L1.B1 (Fig. 15), we look at the position of the collimators that act in the vertical plane, projected into phase space. At the smallest β^* values, losses on TCTPV.4L1.B1 are dominated by particles scattered from the IR7 TCSs with the highest losses coming from TCSG.D4L7.B1. Figure 21 shows the vertical collimators with their phase advance from TCSG.D4L7.B1. It can be seen that, due to the retraction in the jaw gap and change in the phase advance, the TCT is shadowed behind TCLA.C6R7.B1 for β^* of 1 m and larger. In the LHC, TCTPV.4L1.B1 is positioned downstream of TCTPH.4L1.B1, so the BLM will see local showers from the horizontal TCT even when the vertical TCT is not directly hit. This explains the discrepancy between the simulation and BLM data.

With this good modeling of proton losses, we can now use Merlin++ to make predictions for future collimation configuration such as the HL-LHC.

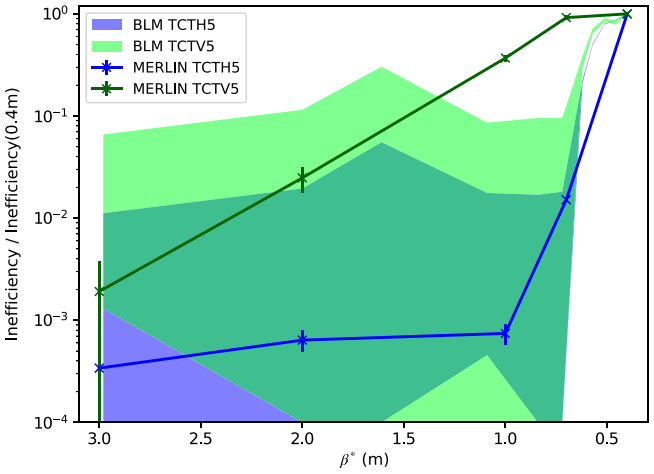

FIG. 17. The BLM signal and Merlin++ simulated losses on IR5 TCTs for horizontal excitation.

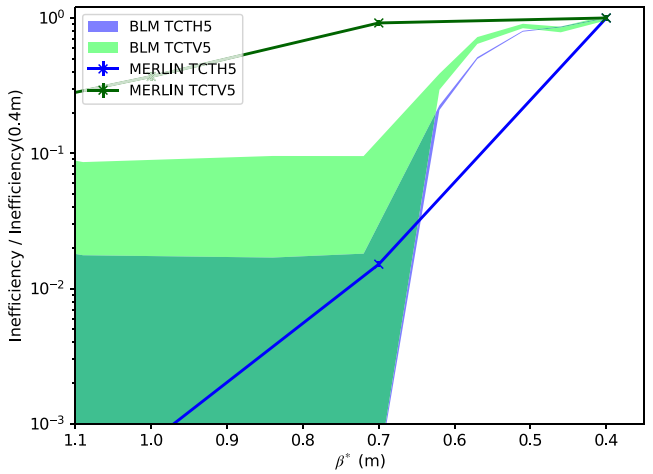

FIG. 18. Enlarged plot of the BLM signal and Merlin++ simulated losses on IR5 TCTs for horizontal excitation.

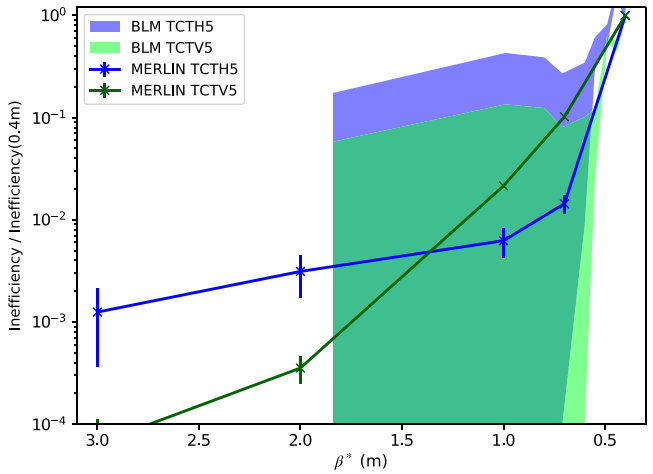

FIG. 19. The BLM signal and Merlin++ simulated losses on IR5 TCTs for vertical excitation.

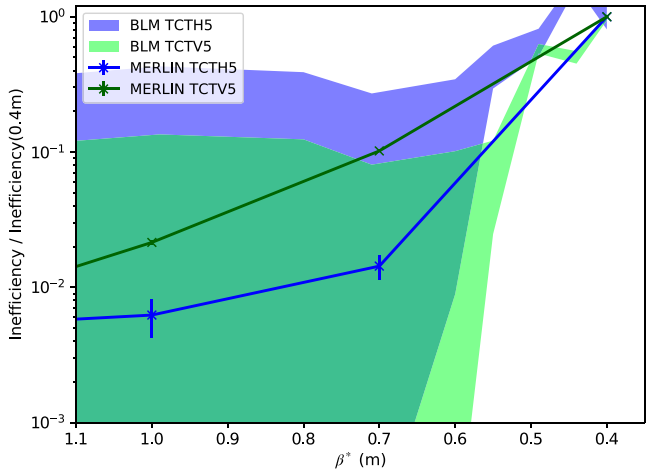

FIG. 20. Enlarged plot of the BLM signal and Merlin++ simulated losses on IR5 TCTs for vertical excitation.

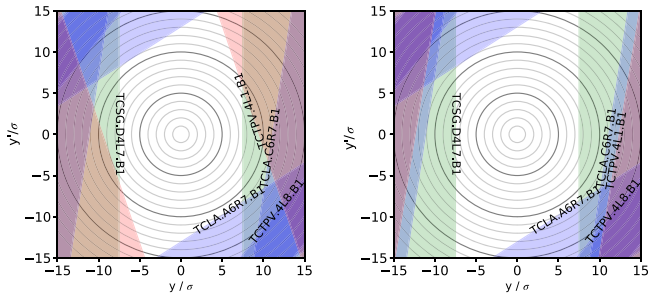

(a) $\beta^* = 40$ cm (b) $\beta^* = 1$ m

FIG. 21. Collimator positions in normalized phase space, accounting for the phase advance from TCSG.D4L7.B1, shown in green, to TCTPV.4L1.B1 shown in red.

TABLE V. Collimator settings for HL-LHC at 7 TeV squeeze from 45 to 15 cm, using a beam emittance of 3.5 μm.

Region	Type	Gap (σ)
IR7	TCP	5.7
IR7	TCS	7.7
IR7	TCLD	12.0
IR3	TCP	15.0
IR3	TCS	18.0
IR1	TCT	18.2 → 10.5
IR5	TCT	18.2 → 10.5
IR2	TCT	30.0
IR8	TCT	30.0

VI. PERFORMANCE OF THE HL-LHC COLLIMATION SYSTEM

The HL-LHC upgrade introduces several changes to the lattice [3]. Among other changes, the inner triplets are replaced with higher-gradient magnets of larger aperture to allow a smaller β^* at the IPs [31], and a new achromatic telescopic squeeze optics scheme is used [32]. In the dispersion matching section downstream of the betatron cleaning, additional absorbers (TCLDs) have been placed by splitting two of the bending magnets into shorter high field magnets [12,14,33]. For each beam in cell 6 upstream of the experiment in IR1 and IR5, an additional pair of TCTs has been placed to improve protection [19].

A. HL-LHC luminosity leveling

In order to maximize integrated luminosity while limiting the maximum pileup, the HL-LHC will use a luminosity leveling scheme [34]. If the accelerator configuration is kept constant during data taking, then the luminosity will fall over the length of the fill due to the gradual reduction in the beam current. Leveling is achieved by adjusting the machine configuration to compensate for the change in the beam current and in the baseline by changing β^* at the IPs.

This leads to another situation where dynamic changes of the collimators could be needed, although in this case with the beams in collision.

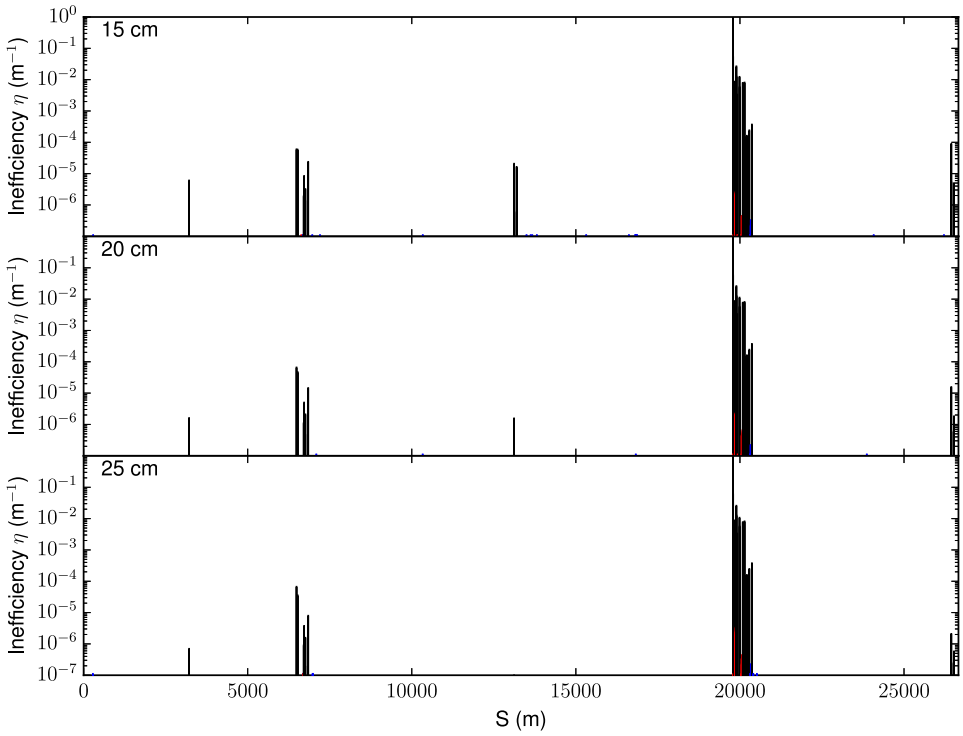

FIG. 22. Merlin++ beam 1 loss map for three IR1/5 β^* value steps during HL-LHC luminosity leveling.

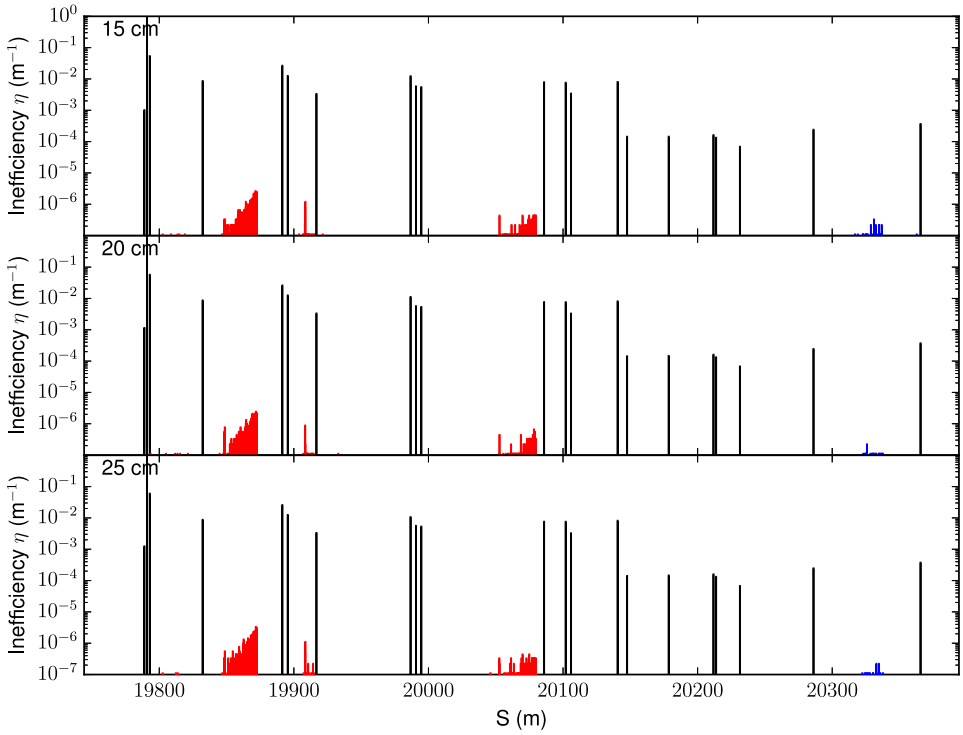

FIG. 23. Merlin++ beam 1 loss map for three IR1/5 β^* value steps during HL-LHC luminosity leveling for IR7.

We consider a leveling scheme that utilizes changes in β^* from 64 to 15 cm while keeping the crossing angle fixed [35]. In this case, the TCTs and TCLs are held at a fixed position in millimeters. The jaws are fixed at the position that gives a TCT gap of 10.5σ and a TCL gap of 12σ at the minimum β^* of 15 cm, using a normalized beam emittance of 3.5 μm. For example, TCTPH.4L1.B1 will have a gap of 15.5 mm for all β^* values. Table V shows the collimator settings used. For this work, we use the HL-LHC version 1.2 optics, with two TCLDs per beam in IR7.

Figures 22 and 23 show the simulated loss map at three steps in the HL-LHC luminosity leveling for the full ring and IR7, respectively. Again, the main losses occur in the collimation regions at IR3 and 7. Smaller loss peaks can also be seen at IR1, 2, and 5. The TCT losses get larger as β^* at the IPs is reduced.

Figures 24 and 25 show the beam 1 losses on the TCTs at the main IPs as a function of the β^* value.

Losses in cold magnets in the rest of the ring are significantly lower than in the LHC configurations due

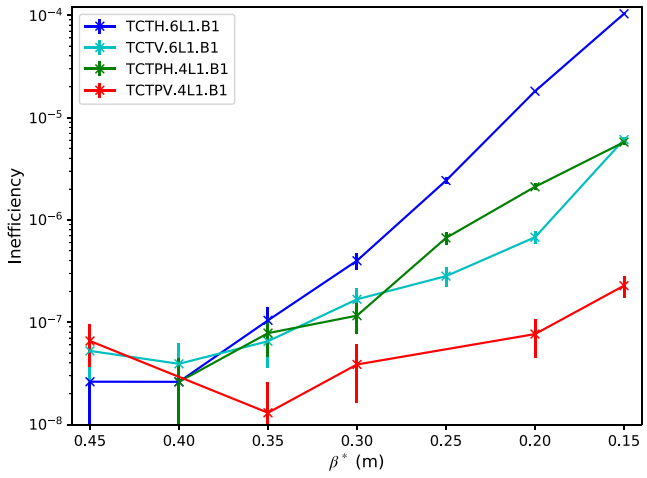

FIG. 24. Merlin++ simulated IR1 TCT losses for horizontal excitation as a function of the β^* value during HL-LHC luminosity leveling.

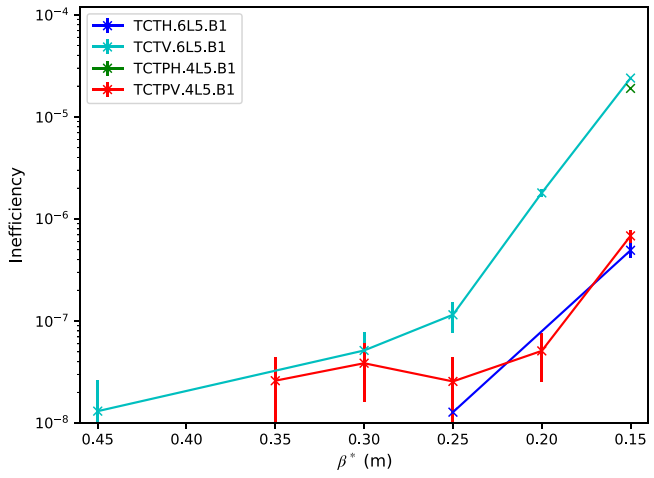

FIG. 25. Merlin++ simulated IR5 TCT losses for horizontal excitation as a function of the β^* value during HL-LHC luminosity leveling.

to the TCLDs catching the dispersive losses. The total cleaning inefficiency of the IR7 collimators at β^* of 45 cm is found to be 7.0×10^{-5} and 6.0×10^{-5} for horizontal and vertical excitation, respectively, and 2.9×10^{-4} and 1.3×10^{-4} at 15 cm. For the horizontal 45 cm case, that is that 99.993% of lost protons are absorbed in the IR7 collimators.

Although there are only very few direct proton losses in cold elements, the showers from the collimators could potentially still quench magnets during the 1 MW loss scenario, but this has been studied with energy deposition studies in Ref. [33]. Studies on the response of the collimators themselves to these loads have been performed in Ref. [36].

VII. CONCLUSION

The LHC collimation system is essential to protect the machine from beam losses during operation. Its performance is continuously monitored by the BLM system. We can use existing measurements to validate simulations, which can then be used to make a prediction of the future performance for HL-LHC.

In this paper, we show that Merlin++ is able to model the proton losses around the LHC. It can reproduce the patterns of losses around the LHC ring and in the interaction regions from measured data. It gives good agreement, to measurements taken with the BLM systems during the beam squeeze, for run 1 and 2 operation at 4 and 6.5 TeV, both in the overall loss patterns and the changes on the TCTs as the optics configuration is changed. The remaining deviations between the simulation and data can be understood by considering the cross talk between elements due to radiation showers which is not included in Merlin++.

In addition to the SixTrack code, already used successfully for collimation studies, we can therefore also use Merlin++ to predict losses in the future HL-LHC configuration. The possibility to use different simulation tools provides increased flexibility and allows estimating systematic uncertainty in the final results. We find that the HL-LHC collimation system performs well with a low cleaning inefficiency. The losses on the cold magnets are acceptable, although the loads in the 1 MW scenario imply also the need of energy deposition studies of the magnet coils, as well as thermomechanical studies of the most loaded collimators.

ACKNOWLEDGMENTS

We thank Alessio Mereghetti, Rogelio Tomas Garcia, and Luis Medina for useful discussion and guidance and Belen Salvachua for BLM data collection. This work is supported by STFC (United Kingdom) grant High Luminosity LHC:UK (HL-LHC-UK), Grant No. ST/N001621/1.

[1] O. S. Brüning, P. Collier, P. Lebrun, S. Myers, R. Ostojic, J. Poole, and P. Proudlock, LHC Design Report v.1: The LHC Main Ring, CERN Yellow Reports: Monographs, CERN, CERN-2004-003-V-1, 2004, http://doi.org/10.5170/CERN-2004-003-V-1.

[2] R. W. Assmann, M. Magistris, O. Aberle, M. Mayer, F. Ruggiero, J. M. Jiménez, S. Calatroni, A. Ferrari, G. Bellodi, and I. Kurochkin, The final collimation system for the LHC, in *Proceedings of the 10th European Particle Accelerator Conference, Edinburgh, Scotland, 2006* (EPS-AG, Edinburgh, Scotland, 2006), p. 986, LHC-PROJECT-Report-919.

[3] G. Apollinari, I. B. Alonso, O. Brüning, P. Fessia, M. Lamont, L. Rossi, and L. Tavian, *High-Luminosity Large Hadron Collider (HL-LHC): Technical Design Report V. 0.1*, CERN Yellow Reports: Monographs Vol. 4 (CERN, Geneva, 2017).

[4] *The High Luminosity Large Hadron Collider: The New Machine for Illuminating the Mysteries of Universe*, edited by O. Brüning and L. Rossi, Advanced Series on Directions in High Energy Physics Vol. 24 (World Scientific, Singapore, 2015), p. 408.

[5] M. Borg, A. Bertarelli, F. Carra, P. Gradassi, J. Guardia-Valenzuela, M. Guinchard, G. Arnau Izquierdo, P. Mollicone, O. Sacristan-de Frutos, and N. Sammut, Thermostructural characterization and structural elastic property optimization of novel high luminosity LHC collimation materials at CERN, Phys. Rev. Accel. Beams **21**, 031001 (2018).

[6] G. Valentino, G. Baud, R. Bruce, M. Gasior, A. Mereghetti, D. Mirarchi, J. Olexa, S. Redaelli, B. Salvachua, A. Valloni, and J. Wenninger, Final implementation, commissioning, and performance of embedded collimator beam position monitors in the Large Hadron Collider, Phys. Rev. Accel. Beams **20**, 081002 (2017).

[7] F. Schmidt, SIXTRACK user's reference manual, Technical Report No. CERN-SL-94-56 (CERN, Geneva, 1994).

[8] SixTrack, 2018, http://sixtrack.web.cern.ch/SixTrack/.

[9] R. Bruce, R. W. Assmann, V. Boccone, G. Bregliozzi, H. Burkhardt, F. Cerutti, A. Ferrari, M. Huhtinen, A. Lechner, Y. Levinsen, A. Mereghetti, N. V. Mokhov, I. S. Tropin, and V. Vlachoudis, Sources of machine-induced background in the ATLAS and CMS detectors at the CERN Large Hadron Collider, Nucl. Instrum. Methods Phys. Res., Sect. A **729**, 825 (2013).

[10] G. Robert-Demolaize, R. Assmann, S. Redaelli, and F. Schmidt, A New Version of SixTrack with Collimation and Aperture Interface, in *Proceedings of the 21st Particle Accelerator Conference, Knoxville, TN, 2005* (IEEE, Piscataway, NJ, 2005), pp. 4084–4086.

[11] R. Bruce, R. W. Assmann, V. Boccone, C. Bracco, M. Brugger, M. Cauchi, F. Cerutti, D. Deboy, A. Ferrari, L. Lari, A. Marsili, A. Mereghetti, D. Mirarchi, E. Quaranta, S. Redaelli *et al.*, Simulations and measurements of beam loss patterns at the CERN Large Hadron Collider, Phys. Rev. ST Accel. Beams **17**, 081004 (2014).

[12] R. Bruce and A. Marsili, and S. Redaelli, Cleaning performance with 11T dipoles and local dispersion suppressor collimation at the LHC, in *Proceedings of the 5th International Particle Accelerator Conference, Dresden,*

Germany, 2014 (JACoW, Geneva, 2014), pp. 170–173, CERN-ACC-2014-0129, MOPRO042, http://doi.org/10.18429/JACoW-IPAC2014-MOPRO042.

[13] P. D. Hermes, R. Bruce, J. M. Jowett, S. Redaelli, B. Salvachua Ferrando, G. Valentino, and D. Wollmann, Measured and simulated heavy-ion beam loss patterns at the CERN Large Hadron Collider, Nucl. Instrum. Methods Phys. Res., Sect. A **819**, 73 (2016).

[14] D. Mirarchi, A. Bertarelli, R. Bruce, F. Cerutt, P. Hermes, A. Lechner, A. Mereghetti, E. Quaranta, S. Redaelli, H. Garcia Morales, R. Kwee-Hinzmann, and R. B. Appleby, Cleaning performance of the collimation system of the High Luminosity Large Hadron Collider, in *Proceedings of the 7th International Particle Accelerator Conference, Busan, Korea, 2016* (JACoW, Geneva, 2016), pp. 2494–2497, WEPMW030, http://doi.org/10.18429/JACoW-IPAC2016-WEPMW030.

[15] R. Bruce, C. Bracco, R. De Maria, M. Giovannozzi, A. Mereghetti, D. Mirarchi, S. Redaelli, E. Quaranta, and B. Salvachua, Reaching record-low β^* at the CERN Large Hadron Collider using a novel scheme of collimator settings and optics, Nucl. Instrum. Methods Phys. Res., Sect. A **848**, 19 (2017).

[16] T. T. Böhlen, F. Cerutti, M. P. W. Chin, A. Fassò, A. Ferrari, P. G. Ortega, A. Mairani, P. R. Sala, G. Smirnov, and V. Vlachoudis, The FLUKA code: Developments and challenges for high energy and medical applications, Nucl. Data Sheets **120**, 211 (2014).

[17] E. B. Holzer, B. Dehning, E. Effinger, J. Emery, G. Ferioli, J. L. Gonzalez, E. Gschwendtner, G. Guaglio, M. Hodgson, D. Kramer, R. Leitner, L. Ponce, V. Prieto, M. Stockner, and C. Zamantzas, Beam loss monitoring system for the LHC, in *Proceedings of the IEEE Nuclear Science Symposium Conference Record, Fajardo, Puerto Rico, 2005* (IEEE, New York, 2005), Vol. 2, pp. 1052–1056, https://doi.org/10.1109/NSSMIC.2005.1596433.

[18] E. B. Holzer, P. Chiggiato, B. Dehning, G. Ferioli, V. Grishin, T. M Jimenez, A. Koshelev, D. Kramer, A. Larionov, M. Taborelli, V. Seleznev, M. Sleptsov, A. Sytin, and I. Wevers, Development, production and testing of 4500 beam loss monitors, in *Proceedings of the 11th European Particle Accelerator Conference, Genoa, 2008* (EPS-AG, Genoa, Italy, 2008), pp. 1134–1136, TUPC037.

[19] S. Redaelli, R. B. Appleby, A. Bertarelli, R. Bruce, J. M. Jowett, A. Lechner, and R. Losito, Cleaning insertions and collimation challenges, in *The High Luminosity Large Hadron Collider: The New Machine for Illuminating the Mysteries of Universe* (World Scientific, Singapore, 2015), pp. 215–241.

[20] R. W. Assmann, I. Baishev, M. Brugger, H. Burkhardt, G. Burtin, B. Dehning, S. Fartouk, C. Fischer, E. Gschwendtner, M. Hayes, J. B. Jeanneret, R. Jung, V. Kain, D. Kaltchev, M. Lamont *et al.*, Preliminary beam-based specifications for the LHC collimators, Technical Report No. LHC-PROJECT-NOTE-277, CERN, 2002.

[21] Merlin developers, Merlin++, 2018, http://www.accelerators.manchester.ac.uk/merlin/.

[22] D. Krücker, F. Poirier, and N. Walker, An ILC main linac simulation package based on MERLIN, in *Proceedings of the 10th European Particle Accelerator Conference, Edinburgh, Scotland, 2006* (EPS-AG, Edinburgh, Scotland, 2006), EUROTEV-REPORT-2006-071, pp. 694–696.

[23] CERN, MADX—Methodical Accelerator Design, 2018, http://mad.web.cern.ch.

[24] J. Molson, Proton scattering and collimation for the LHC and LHC luminosity upgrade, Ph.D. thesis, University of Manchester, 2014.

[25] R. B. Appleby, R. J. Barlow, J. G. Molson, M. Serluca, and A. Toader, The practical Pomeron for high energy proton collimation, Eur. Phys. J. C **76**, 520 (2016).

[26] C. O. Rasmussen and T. Sjöstrand, Models for total, elastic and diffractive cross sections, Eur. Phys. J. C **78**, 461 (2018).

[27] W. Höfle, R. Assmann, S. Redaelli, R. Schmidt, D. Valuch, D. Wollmann, and M. Zerlauth, Controlled Transverse Blow-up of High energy Proton Beams for Aperture Measurements and Loss Maps, in *Proceedings of the 3rd International Particle Accelerator Conference, New Orleans, LA, 2012* (IEEE, Piscataway, NJ, 2012), THPPR039.

[28] G. Valentino and B. Salvachua, Machine learning applied at the LHC for beam loss pattern classification, in *Proceedings of the 9th International Particle Accelerator Conference, Vancouver, British Columbia, 2018* (IEEE, New York, 2018), WEPAF078, https://doi.org/10.18429/JACoW-IPAC2018-WEPAF078.

[29] J. B. Jeanneret, T. Trenkler, L. R. Oberli, and D. Leroy, Quench levels and transient beam losses in LHC magnets, Technical Report No. LHC-Project-Report-44, CERN, 1996.

[30] D. Mirarchi, R. Bruce, M. Fiascaris, P. Hermes, A. Mereghetti, E. Quaranta, S. Redaelli, R. Rossi, B. Salvachua, G. Valentino, A. Valloni, J. Wagner, H. Garcia, and R. Kwee-Hinzmann, Collimation: Experience and performance, in *Proceedings of the 7th Evian Workshop on LHC beam operation*, Evian Les Bains, France, 2016 (CERN, Geneva, Switzerland, 2016), pp. 105–112.

[31] E. Todesco, G. Ambrosio, P. Ferracin, J. M. Rifflet, G. L. Sabbi, M. Segreti, T. Nakamoto, R. Van Weelderen, and Q. Xu, Superconducting Magnet Technology for the Upgrade, in *The High Luminosity Large Hadron Collider: The New Machine for Illuminating the Mysteries of Universe* (World Scientific, Singapore, 2015), pp. 107–135.

[32] S. Fartoukh, Achromatic telescopic squeezing scheme and application to the LHC and its luminosity upgrade, Phys. Rev. ST Accel. Beams **16**, 111002 (2013).

[33] A. Lechner *et al.*, Power deposition in LHC magnets with and without dispersion suppressor collimators downstream of the betatron cleaning insertion, in *Proceedings of the 5th International Particle Accelerator Conference, Dresden, Germany, 2014* (JACoW, Geneva, 2014), pp. 112–115, MOPRO021, https://doi.org/10.18429/JACoW-IPAC2014-MOPRO021.

[34] G. Arduini, M. Lamont, T. Pieloni, and G. Rumolo, Implications for operations, in *The High Luminosity Large Hadron Collider: The New Machine for Illuminating the Mysteries of Universe* (World Scientific, Singapore, 2015), pp. 373–389.

[35] E. Metral, S. Antipov, F. Antoniou, R. B. Appleby, G. Arduini, J. Barranco Garcia, P. Baudrenghien, N. Biancacci,

C. Bracco, R. Bruce, X. Buffat, R. Calaga, L. R. Carver, E. Chapochnikova, M. P. Crouch *et al.*, Update of the HL-LHC operational scenarios for proton operation, Technical Report No. CERN-ACC-NOTE-2018-0002, CERN, 2018.

[36] A. Bertarelli, C. Accettura, E. Berthomé, L. Bianchi, F. Carra, C. Fichera, M. I. Frankl, G. Gobbi, P. Grosclaude, M. Guinchard, A. Lechner, M. Pasquali, S. Redaelli, E. Rigutto, and O. Sacristan De Frutos *et al.*, Dynamic testing and characterization of advanced materials in a new experiment at CERN HiRadMat facility, in *Proceedings of the 9th International Particle Accelerator Conference, Vancouver, British Columbia, Canada, 2018* (IEEE, New York, 2018), WEPMF071, https://doi.org/10.18429/JACoW-IPAC2018-WEPMF071.